Diffusion-advection within dynamic biological gaps driven by structural motion

Robert J. Asaro, Qiang Zhu,* and Kuanpo Lin
Department of Structural Engineering, University of California, San Diego, La Jolla, California 92093, USA

(Received 21 February 2017; revised manuscript received 10 March 2018; published 2 April 2018)

To study the significance of advection in the transport of solutes, or particles, within thin biological gaps (channels), we examine theoretically the process driven by stochastic fluid flow caused by random thermal structural motion, and we compare it with transport via diffusion. The model geometry chosen resembles the synaptic cleft; this choice is motivated by the cleft's readily modeled structure, which allows for well-defined mechanical and physical features that control the advection process. Our analysis defines a Péclet-like number, $\mathcal{A}^D$, that quantifies the ratio of time scales of advection versus diffusion. Another parameter, $\mathcal{A}^M$, is also defined by the analysis that quantifies the full potential extent of advection in the absence of diffusion. These parameters provide a clear and compact description of the interplay among the well-defined structural, geometric, and physical properties *vis-à-vis* the advection versus diffusion process. For example, it is found that $\mathcal{A}^D \sim 1/R^2$, where R is the cleft diameter and hence diffusion distance. This curious, and perhaps unexpected, result follows from the dependence of structural motion that drives fluid flow on R. $\mathcal{A}^M$, on the other hand, is directly related (essentially proportional to) the energetic input into structural motion, and thereby to fluid flow, as well as to the mechanical stiffness of the cleftlike structure. Our model analysis thus provides unambiguous insight into the prospect of competition of advection versus diffusion within biological gaplike structures. The importance of the random, versus a regular, nature of structural motion and of the resulting transient nature of advection under random motion is made clear in our analysis. Further, by quantifying the effects of geometric and physical properties on the competition between advection and diffusion, our results clearly demonstrate the important role that metabolic energy (ATP) plays in this competitive process.

DOI: 10.1103/PhysRevE.97.042401

I. INTRODUCTION

Examples are legion of biological systems in which an exchange of solute and/or solvent across or along the walls of channels or thin gaps, through which fluid solution flows, occurs. This, of course, suggests that advection coupled to diffusion may play an important role in the overall transport. Indeed, this underlies a basis of Starling's hypothesis [1], of over a century ago, that fluid is filtered at the arterial end of a vessel such as a lymphatic vessel, and reabsorbed at the venous end through fluid flow. Advection influences have been assessed within the framework of the *standard gradient* model for water transport, *inter alia* [2,3]. Other examples are found within the Golgi complex, within channels of epithelial cells, and in the thin gaps between cells during their adhesion. Advective flow of potentially toxic metabolic byproducts within the brain has been recently discussed [4]; the concepts proposed there are similar in part to Starling's idea. In the brain, this is thought to occur via the interstitial space and fluid, and although detailed models for this and the energetic sources that drive the process may be yet unknown, evidence for advection versus diffusion is compelling [4]. Combined diffusion and advection occurring within the interstitial space of tissue has been experimentally explored since at least 1989. For example, Chary and Jain [5] measured the transport of bovine serum albumin within chambers implanted in the ears of rabbits. In such cases of larger molecules, experimentally measured diffusion coefficients of order $D \sim 10^{-11}$ m^2 s^{-1} indeed showed that advection contributed a vital role in the overall transport. For later reference, we note that Chary and Jain [5] reported measured fluid velocities in the range $v \sim 0.5{-}0.6$ μm s^{-1}; such velocity range will be referred to below and quite favorably compared to our model's forecasted ranges, say $v \sim 0.5{-}1.0$ μm s^{-1} [see Sec. III C, Eq. (34) and then Sec. III A, Eq. (13)].

These combinations of diffusion coefficient and fluid velocity values demonstrate a definite contribution of advection. To explore this, we consider the example of possible advection coupled to diffusion in the transport of neurotransporters within a synaptic cleftlike geometry (also known as a gap) of nerve dendrites [6,7]. Advection within the synaptic cleft might not be thought of as a major contribution to molecular transport due to its restricted transport distances, $200 \lesssim R \lesssim 1000$ nm, yet it provides a quite clear geometry (Fig. 1) to explain the effects of structural motion that reveals an inverse effect of length scale on transport. For example, with $D \sim 10^{-11}$ m^2 s^{-1}, $R \sim 1$ μm, and $v \sim 5$ μm s^{-1} we find a Peclet number Pe $\sim$ Ru$/D \sim 0.5$ that about brings advection about competitive with diffusion. We explore, however, a vital link between length scale with Pe within our models via predicted fluid-solid interaction; this links length scale with v in an inverse relation. In fact, we introduce a number, $\mathcal{A}^D$, that compares timescales for advection versus diffusion and find $\mathcal{A}^D \sim 1/R^2$. This unexpected result for the effect of diffusion distance is due to the strong R^4 dependence of hydrodynamic resistance of our model rigid disk.

*qizhu@ucsd.edu

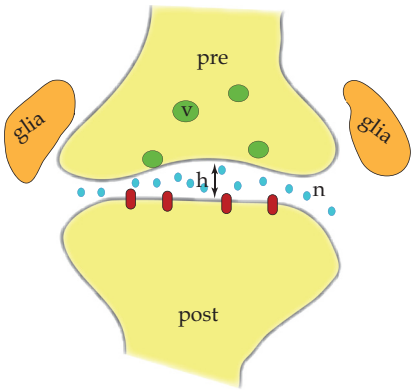

FIG. 1. Schematic of pre- and postsynapses separated by a synaptic cleft (also known as a "gap") of width h. Also indicated are synaptic vesicles that release glutamate into the cleft. Note that the synapse has a glial cell sheath that is not explicitly included in our model.

Of course, the fluid flow considered herein does not compare with that found in *cytoplasmic streaming* in plants discovered over 240 years ago [8,9]. Recent reviews [10,11] discuss fluid velocities well in the range of $v \sim 1-10\ \mu\mathrm{m\,s^{-1}}$, and even as high as $40-60\ \mu\mathrm{m\,s^{-1}}$ [12,13]. The flow is driven by the motion of myosin motor proteins along actin filaments that carry "cargo" consisting, *inter alia*, of vesicles, organelles, and molecular complexes. This, in turn, provides a velocity boundary condition that sets fluid flow patterns throughout the bulk of the cytosol and vacuoles of the plant cell. As Pickard [9] pointed out, however, it may not be the advection of fluid flow *per se* that is responsible for the more critical transport but the "towing" via the myosin carriers of vital entities. Two aspects of cytoplasmic streaming in plants are worth noting here, however. First, the ranges of fluid velocities involved suggest a clear potential for significant contributions of advection *vis-à-vis* diffusion for molecular transport, especially over distances $L \geqslant 1\mu$; indeed this has provided perspective on the limits to animal cell size, as opposed to larger plant cell sizes, if it is assumed that diffusion *per se* is the most viable mode of ion and molecular transport in animal cells [10]. Secondly, is the role of ATP hydrolysis that powers cytoplasmic streaming [10,11]. We will likewise assume that ATP hydrolysis is necessary to achieve sufficient hydrodynamic flow to render advection significant.

As it happens, in biological systems fluid flow is often described as random flow since it is driven by thermal fluctuations; hence the advection flow of solutes within the fluid solutions is a stochastic process. Advection-diffusion precesses have been the subject of various studies in a general context, and it has been shown that under certain circumstances advection can indeed have a significant role as compared to diffusion *per se* [14,15]. Recent experimental evidence has, in fact, been analyzed and reported for stochastic advective transport lysomes in motile neutrophil-like cells coupled to diffusion [16]. In this interesting case, the contributions of diffusion versus stochastically driven advection were separately identified via the characteristically different time dependence of particle trajectories. Advection due to the stochastic fluid motion driven by the shape changes that occurred during the cell's crawling motion was indeed notable with fitted diffusion coefficients of the order of $D \sim 10^{-14}\ \mathrm{m^2\,s^{-1}}$. This result is consistent with our forecasted results as noted in Sec. V. We indeed explore the advection-diffusion coupling during random flow within the basic structure of the synapse cleft. This is to serve as a prototypical case study whose insights should pertain to a wide range of scenarios.

Transport has been analyzed within the synaptic gap [7–17]; such studies have focused on events such as *spillover* [18,19]. For a complete description of the transient distribution of neurotransmitters after release within a geometry such as the synaptic gap, account must be taken of the glial cell coverage around the synapse that may impede extracellular diffusion. Such refinement is not included here where we use a simple boundary condition at the synapse perimeter. Direct observation of the transient transmitter concentration profile has proved elusive, and hence reliance on theoretical modeling has been used for forecasts. To date, modeling has been concerned with analyzing diffusion as the only transport mechanism—clearly this is reasonable since published values for the diffusion coefficients [6,17] would argue for such diffusion's general dominance. However, the influence of advection coupled to diffusion has yet to be explored.

The aim here is to formulate a simple, credible, model for the advection-diffusion process of transport of glutamate or other molecules within the synaptic cleft, or a cleftlike geometry, wherein the various physical features, and individual subprocesses, are well defined and such that each displays a clear role in controlling the overall process. As it happens, there are parameters linked to particular features that control the timescales of advection versus diffusion, and on the other hand parameters that determine the potential magnitude of the advection contribution. The latter parameter is dependent on the energetics driving synaptic motion that causes fluid motion either due to thermal fluctuations and possible metabolic energy sources, e.g., ATP hydrolysis. This is discussed in some detail in Sec. IV A. Thus a main purpose of the model analysis presented herein is to provide a clear model scenario for what determines the role of advection driven by structural motion.

II. PROBLEM DESCRIPTION

The essential geometry of the model, and the boundary-value problem, is illustrated in Fig. 2. A neuron (nu) is located above a dendrite (den) at the instantaneous height $h(t)$. The neuron is modeled as a rigid disk of radius R and of mass m. The neuron is in thermal motion, in the z direction, relative to the dendrite as modeled in the next section. The motion is random, composed of white noise via thermal fluctuations and possible additional metabolic energy input. However, for comparison we shall also consider deterministic motions including harmonic motion. So much for the geometry. We will assume, as detailed below, that the geometry in which $h/R \ll 1$ allows for a thin-film approximation so that concentrations as well as fluid flow can be thought of as z-averaged, or resultant quantities.

At time $t = 0$, a flood of neurotransmitters is ejected into the synapse gap creating an initial concentration, $c(r,0) = c_0$; the concentration of neurotransmitters outside the gap is zero. One simple boundary condition to account for this is to set $c(R,t) = 0$. For the synapse, such a boundary condition may

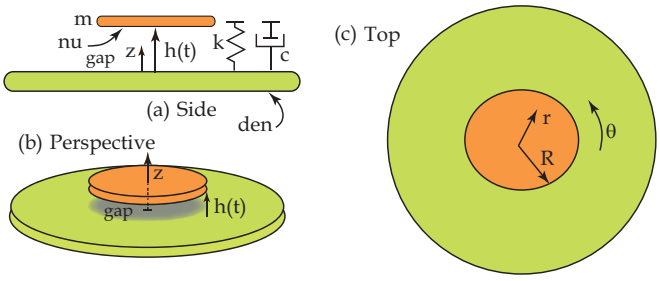

FIG. 2. The synapse is modeled as a disk (nu) oscillating above a fixed half-plane (den) and restrained by a linear spring (k) and subject to a linear viscous drag (c). See also Fig. 3 and its associated discussion for additional details. Figure 5 shows an alternative model involving two opposing disks; the associated discussion explains that these two models are essentially equivalent.

arise via the absorption of neurotransmitters by the glial cells located at the periphery of the cleft (Fig. 1 and [18]). This sort of model does require further discussion, however, as given below.

To model the motion of the disk above its substrate, we couple it via a linear spring representing a harmonic potential and a damper that is meant to account for viscous frictional resistance of the surrounding fluid. This is depicted in Fig. 2(a), the side view of the system.

The idea is this: the motion of the disk induces a Stokes fluid flow field whose through thickness average radial component takes the form

$$\bar{v}_r = -\frac{1}{2h}\frac{dh}{dt}r. \tag{1}$$

As dh/dt oscillates in sign, fluid flows out of and into the gap carrying solute via both diffusion and advection. When fluid flows out of the gap, which is at a higher concentration, the concentration outside is increased, whereas when fluid flows into the gap its concentration is lower than c_0. One may expect that the net effect is to reduce the gap concentration via advection. Of course, diffusion will also have the effect of reducing the gap concentration as well. The effect of advection may then be an enhancement of solute transport. However, this will be dependent on the temporal pattern of the fluid flow as created by the disk's motion. For example, recall that the assumed well-ordered Stoke's flow is *reversible* (e.g., [20–22]). Hence, if the disk's motion is, say, harmonic, then the advection effects will vanish since the same volume elements of fluid with their solute will be reversibly transferred into and out of the gap over a period of motion. In such cases, mixing of solute occurs only via diffusion. Indeed, this is similar to a simple particle random walk or to Brownian particle motion whereby unbiased random jumps lead to a time-average distance, r, traveled $\langle r\rangle = 0$ (hereby $\langle\,\rangle$ refers to an average in time) yet to a mean-square distance $\langle r^2\rangle \propto t$. As shown in Secs. III B and III C, if $h(t) = h_0 + \eta(t)$, where $\eta(t)$ is a random motion about a mean gap width h_0, the time average $\langle d\eta^2/dt\rangle$ controls the time average of advective flow. Hence our case of a stochastically driven flow field is not a case of a smooth reversible flow. As particles in a stochastic Brownian motion are subject to randomly imposed forces, solute particles here are subject to a randomly imposed fluid flow field that results in net diffusivelike transport [23] (see especially Chap. VIII, Sec. 3).

The above considerations suggest that to observe an advection effect, the motion must somehow be biased and irregular. In fact, the motion of biological membranes is commonly driven by thermal fluctuations and hence is random. We explore this using a familiar mechanical model for such motion. We also confirm our comments concerning regular motion by setting

$$h(t) = h_0 + a\sin\omega t \quad \text{with } h_0 > 0, |a| < h_0. \tag{2}$$

We note that a similar model has been proposed by Pannuzzo *et al.* [24], and here we carry such analysis further. Our mathematical development is, however, quite different, as are our conclusions.

III. MATHEMATICAL FORMULATIONS

A. Fluid flow field

The relevant equations for Stokes flow are

$$0 = -\nabla p + \mu\nabla^2\mathbf{v} \quad \text{with } \nabla\cdot\mathbf{v} = \mathbf{0}, \tag{3}$$

with $\mathbf{v}$ being the fluid velocity and μ the fluid viscosity. Geometry suggests that $\mathbf{v}$ is of the form

$$\mathbf{v} = v_r\mathbf{e}_r + v_z\mathbf{e}_z, \tag{4}$$

with $\mathbf{e}_r$ and $\mathbf{e}_z$ unit base vectors, and $v_\theta = \partial(\,)/\partial\theta = 0$ by radial symmetry. Dimensional analysis, noting that $h/R \ll 1$, leads to the typical *thin-film* approximation [20] of Eq. (3), viz.,

$$\frac{\partial p}{\partial r} = \mu\frac{\partial^2 v_r}{\partial z^2}. \tag{5}$$

Integrating Eq. (5) yields

$$v_r = \frac{1}{2\mu}\frac{\partial p}{\partial r}z(z-h), \tag{6}$$

since no-slip conditions demand, even within the thin-film approximation, that $v_r = 0$ for $z = 0,h$ [20,22,25]. Now use $\nabla\cdot\mathbf{v} = \mathbf{0}$ in cylindrical coordinates to obtain

$$\frac{1}{r}\frac{\partial}{\partial r}(rv_r) + \frac{\partial v_z}{\partial z} = 0, \tag{7}$$

and then

$$v_z = -\frac{1}{2\mu r}\frac{\partial}{\partial r}\left(r\frac{\partial p}{\partial r}\right)\left\{\frac{z^3}{3} - \frac{z^2}{2}\right\}. \tag{8}$$

Since $v_z(z=h) = dh/dt$, we find from Eq. (7)

$$\frac{\partial}{\partial r}\left(r\frac{\partial p}{\partial r}\right) = \frac{12\mu r}{h^3}\frac{dh}{dt}, \tag{9}$$

which when substituted back into Eq. (8) yields

$$v_z = -6\frac{dh}{dt}\left\{\frac{1}{3}\left(\frac{z}{h}\right)^3 - \frac{1}{2}\left(\frac{z}{h}\right)^2\right\}. \tag{10}$$

Now from Eq. (9) we find, upon integration,

$$\frac{\partial p}{\partial r} = \frac{6\mu r}{h^3}\frac{dh}{dt} + \frac{y(t)}{r}, \tag{11}$$

whence, using Eq. (6),

$$v_r = -3\,\frac{1}{h}\,\frac{dh}{dt}\,r\left\{\left(\frac{z}{h}\right)-\left(\frac{z}{h}\right)^2\right\}. \tag{12}$$

In Eq. (11), $y(t)=0$ since no singularity is allowed.

At this point, we again appeal to a thin-film approximation [20,22] and define a through thickness average radial velocity component,

$$\bar{v}_r = \frac{1}{h}\int_0^h v_r dz = -\frac{1}{2h}\,\frac{dh}{dt}\,r. \tag{13}$$

We also note from Eqs. (10) and (12) that v_r/v_z scales as Rh^{-1} and thus the thin-film approximation would justify ignoring v_z as compared to v_r [20,22].

Incidently, the synapse can be alternatively modeled as two opposing identical disks. Details about the fluid dynamics of this system are included in Appendix A.

For later reference, we also compute the pressure within the gap by integrating Eq. (11) to obtain

$$p = \frac{3\mu}{h^3}\,\frac{dh}{dt}\,r^2 + f(t), \tag{14}$$

whereupon we note that at $r=R$, $p=p_0$, the outside pressure. Hence

$$p(r) = p_0 + \frac{3\mu}{h^3}\,\frac{dh}{dt}\,(r^2-R^2). \tag{15}$$

Then form the area integrated pressure difference $p-p_0$, i.e.,

$$\begin{aligned} f &= \int_0^{2\pi}\int_0^R \{p(r)-p_0\}\,r\,dr\,d\theta \\ &= -\frac{3\pi\mu}{2}\,\frac{R^4}{h^3}\,\frac{dh}{dt} = -\xi\,\frac{dh}{dt}. \end{aligned} \tag{16}$$

The force f is a resistive force, or adhesive force, resisting disk motion. For later use we note that

$$\xi = \frac{3\pi\mu}{2}\,\frac{R^4}{h^3} \tag{17}$$

serves as a *friction coefficient*. We note that this result for the drag coefficient may be extracted from Davis' analysis [26] of sedimentation of disklike particles approaching a rigid plane in the limit where $h/R \ll 1$. The fluid velocity field is not readily extracted as hence is developed here.

B. Random vibration of the membrane disk

As described in Fig. 2(a), our model for the disk is the all too familiar damped oscillator attached to a linear spring, k, and damper, c. We dub $\omega_0^2 = k/m$ and $\gamma = c/m$, where m is the disk's mass. We assume, as our numerics for the physical parameters later describes, that $\gamma^2/4 \gg \omega_0^2$, i.e., an overdamped regime. We let $h(t) = h_0 + \eta(t)$, where h_0 is the average and rest elevation of the disk. Let the disk be driven by a random force, $\mathcal{F}(t)$, caused by thermal fluctuations. This random force can be quantified by coupling the disk system to a heat bath. Hence one model for $\mathcal{F}(t)$, or $\eta(t)$, is as a Gaussian white noise variable with a δ correlation satisfying $\langle \mathcal{F}(t_1)\mathcal{F}(t_2)\rangle = \Gamma\delta(t_2-t_1)$, with Γ the strength of the force.

However, we note that the mechanical model for our structural system shown in Fig. 2 presents constraints on $h(t)$. For example, we require $|\eta(t)| < h_0$, as clearly $h(t) > 0$. To handle such constraints, we may postulate that $\mathcal{F}(t)$, and later $\eta(t)$, be described as *random telegraph noise* [27] where, for example, $\eta(t)$ transitions between $\eta = -s$ to s and $\eta = s$ to $-s$, $0 \leqslant s < h_0$, with rates ν_1 and ν_2, respectively. This means that the fractions of time spent in gap compression and opening modes are $\nu_2/(\nu_1+\nu_2)$ and $\nu_1/(\nu_1+\nu_2)$, respectively. The telegraph noise fluctuations of $\eta(t)$ are correlated as

$$\langle \eta(t_1)\eta(t_2)\rangle = \frac{4s^2\nu_1\nu_2}{\nu^2}\,e^{-\nu|t_1-t_2|}, \tag{18}$$

with $\nu = \nu_1+\nu_2$, a smoother transition than the δ correlation of Gaussian white noise. For straightforward connection of our system to a thermal heat bath, as we do below, we will take $\Delta\nu = \nu_2-\nu_1 = 0$, which yields

$$\langle \eta(t_1)\eta(t_2)\rangle = s^2 e^{-\nu|t_1-t_2|} \;\rightsquigarrow\; \langle \eta^2(t)\rangle = s^2. \tag{19}$$

We also note that, as with Gaussian white noise, we will have with $\Delta\nu = 0$

$$\langle \eta(t)\rangle = -s\,\frac{\Delta\nu}{\nu} = 0. \tag{20}$$

For future reference, and study, we observe that with nonzero $\Delta\nu$, say $\Delta\nu > 0$, we would be describing scenarios in which the gap spends more time in compression than in an opening mode; the opposite will be true if $\Delta\nu < 0$. For now, we emphasize that with the view just presented above, we will have $|\eta(t)| < h_0$ and hence $h(t) > 0$. This is important for the development of Sec. III C to follow.

With either view for the stochastic description, the equation of motion is

$$\frac{d^2\eta}{dt^2} + \gamma\,\frac{d\eta}{dt} + \omega_0^2\eta = \frac{\mathcal{F}(t)}{m}. \tag{21}$$

Recall that γ is from the previous section, i.e., Eq. (17),

$$\gamma = \frac{\xi}{m} = \frac{3\pi\mu}{2m}\,\frac{R^4}{h^3} \;\rightsquigarrow\; \gamma \approx \frac{3\pi}{2m}\,\frac{R^4}{h_0^3}\,\mu. \tag{22}$$

The second of Eq. (22) aims to linearize Eq. (21) in the range where $|\eta| \ll h_0$. As $\eta(t)$ is a random motion, driven by $\mathcal{F}(t)$, its average is $\langle \eta(t)\rangle = 0$.

The resolution of Eq. (21) follows standard lines as in Brownian motion [28], e.g., begin by multiplying through by η to obtain

$$\eta\,\frac{d^2\eta}{dt^2} + \gamma\,\eta\,\frac{d\eta}{dt} + \omega_0^2\eta^2 = \eta\,\frac{\mathcal{F}(t)}{m}, \tag{23}$$

and note that

$$\begin{aligned} \eta\,d\eta/dt &= 1/2\,d\eta^2/dt \;\text{ and} \\ \eta\,d^2\eta/dt &= 1/2\,d^2\eta^2/dt^2 - (d\eta/dt)^2. \end{aligned} \tag{24}$$

This leads to

$$\frac{d^2\eta^2}{dt^2} + \gamma\,\frac{d\eta^2}{dt} + \omega_0^2\eta^2 = 2\left(\frac{d\eta}{dt}\right)^2 + \eta\,\frac{\mathcal{F}(t)}{m}. \tag{25}$$

Now take time-average values across Eq. (25) to obtain

$$\frac{d^2\langle\eta^2\rangle}{dt^2}+\gamma\frac{d\langle\eta^2\rangle}{dt}+\omega_0^2\langle\eta^2\rangle = 2\left\langle\left(\frac{d\eta}{dt}\right)^2\right\rangle+\left\langle\eta\frac{\mathcal{F}(t)}{m}\right\rangle. \tag{26}$$

Note that as η and $\mathcal{F}$ are uncorrelated, the last term is zero since $\langle\eta\rangle=0$. To connect our disk to a heat bath, invoke the equipartition theorem [28,29] to obtain

$$\frac{d^2\langle\eta^2\rangle}{dt^2}+\gamma\frac{d\langle\eta^2\rangle}{dt}+\omega_0^2\langle\eta^2\rangle = 2\frac{kT}{m}. \tag{27}$$

The next step is to make a change of variables and set $\langle\eta^2\rangle = q(t)e^{-\gamma t/2}$, which leads to

$$\frac{d^2q}{dt^2}+\left(\omega_0^2-\gamma^2/4\right)q=\frac{2kT}{m}e^{\gamma t/2}. \tag{28}$$

We choose a simple and convenient set of initial conditions that ensure that $q>0$, viz., $\langle\eta^2(0)\rangle = 2kT/\omega_0^2$ and $d\langle\eta(0)\rangle dt = 0$. The solution is

$$\langle\eta^2\rangle(t)=\frac{2kT}{m\omega_0^2}\left\{\cosh(\zeta t)+\frac{\gamma}{2\zeta}\sinh(\zeta t)\right\}e^{-\gamma t/2}+\frac{2kT}{m\omega_0^2}, \tag{29}$$

with $\zeta=(\gamma^2/4-\omega_0^2)^{1/2}$.

The trailing constant in Eq. (29) is a long time, i.e., stationary, solution in that if, as we assume, $\gamma^2/4\gg\omega_0^2$,

$$\langle\eta^2\rangle(t\to\infty)\to\frac{2kT}{m\omega_0^2}. \tag{30}$$

To obtain this required analytic solution, we have not constrained the amplitudes of motion of our mechanical model of Fig. 2. We nonetheless note that within the entire range of values for physical parameters described later, we indeed find that $\langle|\eta^2(t)|\rangle < h_0^2$.

C. The random flow field

For the flow field of Eq. (13) we need the following quantity, and we note that

$$\frac{1}{h}\frac{dh}{dt}=\frac{1}{2h^2}\frac{dh^2}{dt}=\frac{1}{h}\frac{d\eta}{dt}. \tag{31}$$

On the other hand, we also note that $h^2=h_0^2+2h_0\eta+\eta^2$ leads to

$$\frac{dh^2}{dt}=2h_0\frac{d\eta}{dt}+\frac{d\eta^2}{dt},\quad\text{whereby}$$
$$\frac{d\eta}{dt}=h_0\frac{1}{h}\frac{d\eta}{dt}+\frac{1}{2h}\frac{d\eta^2}{dt}. \tag{32}$$

Now realizing that both $\langle n(t)\rangle=0$ and $\langle d\eta/dt\rangle=0$, when average values are taken across the second of Eq. (32) we find that

$$\left\langle\frac{1}{h}\frac{d\eta}{dt}\right\rangle=-\frac{1}{2h_0}\left\langle\frac{1}{h}\frac{d\eta^2}{dt}\right\rangle\approx-\frac{1}{2h_0^2}\left\langle\frac{d\eta^2}{dt}\right\rangle. \tag{33}$$

Recall that we have set things up so that $h(t)=h_0+\eta(t)>0$, which helps justify the above approximation. Using Eq. (29), we find

$$\left\langle\frac{1}{h}\frac{d\eta}{dt}\right\rangle\approx\frac{kT}{m\gamma h_0^2}e^{-\omega_0^2t/\gamma}. \tag{34}$$

We note that when this is used with Eq. (13) we find that the forecasted radial fluid velocities are of order $0.5-1.0\ \mu\mathrm{m\,s}^{-1}$ as was coincidentally found to be representative in the experimental study of Chary and Jain [5], and as was mentioned in the first paragraph of Sec. I.

D. Diffusion-advection equation and its solution

The diffusion-advection equation reads as follows:

$$\frac{\partial c}{\partial t}=D\nabla^2c-\nabla\cdot(c\mathbf{v}), \tag{35}$$

where c is the concentration, D is the diffusion coefficient, and $\mathbf{v}$ again is the fluid velocity. We will transform this to a purely radial equation as follows. To begin, we note that we have assumed radial symmetry, hence $c=c(r,z)$, $\mathbf{v}=\mathbf{v}(r,z)$. Recall the definition within the thin-film approximation of $\bar{v}_r$ in Eq. (13). The diffusion term involving ∇^2c will be clear enough, but attention to the advective term requires comment.

In cylindrical coordinates, and in component form,

$$\nabla\cdot(c\mathbf{v})=\frac{1}{r}\frac{\partial}{\partial r}(rv_rc)+\frac{1}{r}\frac{\partial(cv_\theta)}{\partial\theta}+\frac{\partial(cv_z)}{\partial z}. \tag{36}$$

Carrying out the operations and grouping terms into two groups, we find

$$\nabla\cdot(c\mathbf{v})=c\frac{1}{r}\frac{\partial}{\partial r}(rv_r)+c\frac{1}{r}\frac{\partial v_\theta}{\partial\theta}+c\frac{\partial v_z}{\partial z}\ (=0)$$
$$+v_r\frac{\partial c}{\partial r}+\frac{v_\theta}{r}\frac{\partial c}{\partial\theta}+v_z\frac{\partial c}{\partial z}\ (\neq 0). \tag{37}$$

The first group is zero since, in this case, $\nabla\cdot\mathbf{v}=\mathbf{0}$. The second term in the second group is zero due to radial symmetry. Hence

$$\nabla\cdot(c\mathbf{v})=v_r\frac{\partial c}{\partial r}+v_z\frac{\partial c}{\partial z}. \tag{38}$$

Now again in the spirit of our thin-film approximation, we define $\bar{c}$ as

$$\bar{c}(r)=\int_0^h c(r,z)dz; \tag{39}$$

hence $\partial\bar{c}/\partial z=0$. Thus

$$\nabla\cdot(\bar{c}\mathbf{v})=\bar{v}_r\frac{\partial\bar{c}}{\partial r}. \tag{40}$$

The diffusion-advection equation thus reads

$$\frac{\partial\bar{c}}{\partial t}=D\nabla_r^2\bar{c}-\bar{v}_r\frac{\partial\bar{c}}{\partial r}\quad\text{with}\quad\nabla_r^2=\frac{\partial^2}{\partial r^2}+\frac{1}{r}\frac{\partial}{\partial r}. \tag{41}$$

Recalling Eq. (13), Eq. (41) reads, with Eq. (34), as

$$\frac{\partial\bar{c}}{\partial t}=D\nabla_r^2\bar{c}+\frac{1}{2}\left(\frac{1}{h}\frac{dh}{dt}\right)r\frac{\partial\bar{c}}{\partial r}, \tag{42a}$$

$$\frac{\partial\bar{c}}{\partial t}=D\nabla_r^2\bar{c}+\frac{1}{2}\frac{kT}{m\gamma h_0^2}e^{-\omega_0^2t/\gamma}r\frac{\partial\bar{c}}{\partial r}. \tag{42b}$$

E. Resolution of Eq. (42)

The boundary condition $c(R,t) = 0$, now $\bar{c}(R,t) = 0$, suggests a separated solution of the form

$$\bar{c}(r,t) = \sum_{m=1}^{\infty} A_m(t) J_0(\lambda_m r), \tag{43}$$

where the λ_m are chosen such that $\lambda_m R$ are the zeros of the Bessel function $J_0(x)$, that is, $\lambda_m R = 2.404\,83, 5.520\,08, \ldots (m - 1/4)\pi$ for $m \gg 1$. With this, there is the orthogonality condition

$$\int_0^R J_0(\lambda_m r) J_0(\lambda_n r)\, r\, dr = \begin{cases} 1/2 R^2 J_1^2(\lambda_n R), & m = n, \\ 0, & m \neq n. \end{cases} \tag{44}$$

Equation (42b) is rewritten as

$$\frac{\partial \bar{c}}{\partial t} - D\nabla_r^2 \bar{c} - \frac{1}{2}\frac{kT}{m\gamma h_0^2} e^{-\omega_0^2 t/\gamma}\, r \frac{\partial \bar{c}}{\partial r} = 0. \tag{45}$$

The procedure is standard, namely multiply through Eq. (45) by $r J_0(\lambda_n r)$ and integrate over the range $[0, R]$ using Eq. (44); we note, however, that the third term in Eq. (45) would be handled by first using the fact that

$$r\frac{\partial}{\partial r} J_0(\lambda_m r) = \lambda_m \frac{\partial}{\partial \lambda_m} J_0(\lambda_m r). \tag{46}$$

This brings us to a critical step in which

$$\frac{\partial}{\partial \lambda_n} J_1^2(\lambda_n R) = 2 J_1(\lambda_n R)\{R J_0(\lambda_n R) - R/(\lambda_n R) J_1(\lambda_n R)\}, \tag{47}$$

where, of course, the first term in the curly brackets is zero since $J_0(\lambda_n R) = 0$.

When the terms are assembled, we arrive at the ODE for $A_n(t)$, viz.,

$$A_n'(t) + \left\{\lambda_n^2 D + \frac{kT}{m\gamma h_0^2} e^{-\omega_0^2 t/\gamma}\right\} A_n(t) = 0 \text{ or} \tag{48a}$$

$$A_n'(t) + \left\{\lambda_n^2 D + \beta e^{-st}\right\} A_n(t) = 0 \text{ with} \tag{48b}$$

$$\beta = \frac{kT}{m\gamma h_0^2} \text{ and } s = \omega_0^2/\gamma. \tag{48c}$$

The solution to Eq. (48b) is

$$A_n(t) = A_n^{\circ} \exp\left(-\lambda_n^2 D t + \beta/s e^{-st}\right) \tag{49a}$$

$$\text{with } A_n^{\circ} = A_n(0) e^{-\beta/s} \tag{49b}$$

$$A_n(t) = A_n(0) e^{-\beta/s} \exp\left(-\lambda_n^2 D t + \beta/s e^{-st}\right). \tag{49c}$$

The coefficients $A_n(0)$ are determined from the initial condition

$$c_0 = \sum_{n=1}^{\infty} A_n(0) J_0(\lambda_n r), \tag{50}$$

which leads to

$$A_n(0) = \frac{2c_0}{(\lambda_n R) J_1(\lambda_n R)}. \tag{51}$$

Thus we find

$$\frac{\bar{c}}{c_0} = \sum_{n=1}^{\infty} \frac{2}{(\lambda_n R) J_1(\lambda_n R)} e^{-\beta/s} \exp\left(-\lambda_n^2 D t + \beta/s e^{-st}\right) \times J_0(\lambda_n r), \tag{52a}$$

$$\tilde{c} = \frac{\bar{c}}{c_0} = e^{-\beta/s} \exp(\beta/s e^{-st}) \sum_{n=1}^{\infty} \frac{2 e^{-\lambda_n^2 D t}}{(\lambda_n R) J_1(\lambda_n R)} \times J_0(\lambda_n r). \tag{52b}$$

A simple yet informative way to visualize this solution is to compute an area average of $\tilde{c}$; for this we need

$$\frac{1}{\pi R^2} \int_0^{2\pi} \int_0^R J_0(\lambda_n r) d\theta\, r\, dr = \frac{2}{\lambda_n R} J_1(\lambda_n R), \tag{53}$$

which when used with Eq. (52b) yields

$$\langle \tilde{c} \rangle = e^{-\beta/s} \exp(\beta/s e^{-st}) \sum_{n=1}^{\infty} \frac{4}{(\lambda_n R)^2} e^{-\lambda_n^2 D t}, \tag{54}$$

where here the averaging $\langle\,\rangle$ denotes that average taken in Eq. (53). Indeed, when $t = 0$, we find $\langle \tilde{c} \rangle = 1$ since

$$4 \sum_{n=1}^{\infty} \frac{1}{(\lambda_n R)^2} = 1, \tag{55}$$

and recalling that the $\lambda_n R$ are the zeros of $J_0(x)$.

It is of interest to explore a few limits of Eq. (54). For example, and obviously, when $t \to \infty$ and $D \neq 0$, $\langle \tilde{c} \rangle \to 0$ since diffusion guarantees this given the boundary condition $c(R,t) = 0$. More revealing, however, is the case in which we set $D = 0$ and thus suppress diffusion, leaving only advection to transport solute. In this case, Eq. (54) reads

$$\langle \tilde{c} \rangle = e^{-\beta/s} \exp(\beta/s e^{-st}) \underset{t\to\infty}{\rightsquigarrow} \langle \tilde{c} \rangle = e^{-\beta/s}, \tag{56}$$

given Eq. (55). Since $\beta/s > 0$, we see that advection indeed leads to a reduction in average solute concentration. Moreover, we note that the effects of advection are transient, and they are focused on the initial time of the transport event.

Inspection of the simple results in Eqs. (54) and (56) reveals some key aspects of the advection-diffusion coupling. Clearly the time scales for the two processes can be quite different. For advection, s determines the time scale, whereas for diffusion the exponents $\lambda_n^2 D$ determine timescales. If advection is to couple to, i.e., compete, diffusion s should be comparable to the $\lambda_n^2 D$, or at least to $\lambda_1^2 D$, where $\lambda_1 = 2.404\,83/R$ is the first eigenvalue of $J_0(x)$. Thereby we define $\mathcal{A}^D \equiv s/\lambda_1^2 D$ as a sort of Peclet number.

We note here that the "inverse problem" is of value and is readily generated from the above solution; the inverse is defined so that the initial concentration is zero within the gap and c_0 outside. Detailed formulations are included in Appendix B.

F. Regular disk motion: e.g., harmonic motion

Recall, even before exploring more detailed results, that Eq. (54) is based on a model that describes random motion of the disk and its induced fluid flow field. It is important to note this with respect to the reversibility of Stokes flow as

discussed in connection with Eq. (2). Specifically, consider such harmonic motion that would specify

$$h(t) = h_0 + a\sin\omega t \quad \text{with} \tag{57a}$$

$$\frac{1}{h}\frac{dh}{dt} = \frac{d\ln h}{dt} = \frac{a\omega\cos\omega t}{h_0 + a\sin\omega t}. \tag{57b}$$

When Eq. (57b) is used in Eq. (48b) instead of βe^{-st}, we find the following. Consider the ODE,

$$A_n'(t) + p(t)A_n(t) = 0, \tag{58}$$

and its solution,

$$A_n(t) = A_n^\circ \exp\left\{-\int^t p(t)dt\right\}. \tag{59}$$

In our case,

$$p(t) = \lambda_n^2 D + \frac{1}{h}\frac{dh}{dt} = \lambda_n^2 D + \frac{d\ln h}{dt}. \tag{60}$$

The solution to Eq. (59) with Eq. (60) is

$$A_n(t) = A_n^\circ\left(\frac{1}{h_0 + a\sin\omega t}\right)e^{-\lambda_n^2 Dt}. \tag{61}$$

Dimensional consistency is attained when we realize that $A_n(0) = A_n^\circ/h_0$, hence

$$A_n(t) = A_n(0)\left(\frac{h_0}{h_0 + a\sin\omega t}\right)e^{-\lambda_n^2 Dt}, \tag{62}$$

where $A_n(0)$ is obtained via the initial condition as in Eqs. (50) and (51).

Within the context of the simple model posed herein, the result of Eq. (62) concerning the advection would go something like this: *what goes out, comes back in*. This arises due to the reversibility of Stokes flow [20,21] when dealing with smooth reversible fluid flow. We recall, however, that the time average of the advection flow field is driven by the average quantity $\langle h^{-1}d\eta/dt\rangle$ that we have shown in Secs. III B and III C to be nonzero, yet decaying exponentially in time. Fluid flow in this case is not a smooth reversible flow but is stochastic in nature, and hence such simple reversibility does not apply [15].

IV. RESULTS

A. Numerics for parameters

Figures 1 and 3 illustrate key structural features of the synapse cleft (i.e., gap) and the release of neurotransmitters. From Savtchenko and Rusakov [6] we note the following dimensions (see also Fig. 2): $150 \leqslant R \leqslant 300$ nm and $12.5 \leqslant h_0 \leqslant 20$ nm. We take the viscosity, μ, to be in the range $\sim 10^{-3}$ Ns m^{-2} [18]. For the mass, m, we use the range $10^{-15} \leqslant m \leqslant 10^{-15}$ kg. This places γ, as per Eq. (22), in the approximate range $10^8 \leqslant \gamma \leqslant 10^9$ s^{-1}. For D we use values in the range $10^{-12} \leqslant D \leqslant 10^{-9}$ m^2 s^{-1}; this includes the range identified for glutamate within the synaptic cleft [6,17].

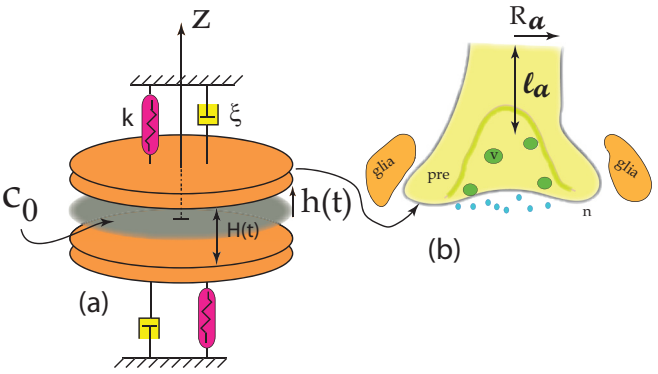

FIG. 3. The synapse is modeled with more detail as a disk attached to a segment of axon that acts as a linear spring with constant $k = E\pi R_a^2/\ell_a$. The motion of the disk is also resisted by a viscous drag coefficient, ξ, given by Eq. (17) and a damping coefficient, γ, given in Eq. (22).

The key parameters within Eqs. (52a), (52b), (54), and (56) can be summarized as

$$\beta = \frac{\alpha kT}{m\gamma h_0^2}, \quad s = \frac{\omega_0^2}{\gamma}, \quad \beta/s = \frac{\alpha kT}{m\,\omega_0^2 h_0^2},$$
$$\omega_0^2 = \frac{E\pi R_a^2}{\ell_a m}, \quad \gamma = \frac{3\pi}{2m}\frac{R^4}{h_0^3}\mu. \tag{63}$$

We note that the scaling parameter α equals unity for thermal fluctuations alone, as was originally envisioned in Eq. (27). However, suppose that we allow for the inclusion of additional energy input, e.g., from ATP hydrolysis that is known to occur in the process of vesicle release and recycling in the synapse [30,31]. For perspective, recall that the standard free energy of ATP hydrolysis is $\Delta G = -30.5$ kJ mol^{-1}. This translates to $\Delta g \approx -12kT$ per molecule. Moreover, with typical cell concentrations $c_{\rm ATP} = 3$ mM, $c_{\rm ADP} = 0.8$ mM, $c_{P_i} = 4$ mM [32], a simple calculation, for the reaction $\mathrm{ATP} + \mathrm{H_2O} \leftrightarrows \mathrm{ADP} + \mathrm{P}_i$, shows that $\Delta G = -48.1$ kJ mol^{-1}, i.e., $\Delta g \approx -19kT$ per molecule. Indeed, for some time now vibrations of microtubules and actin filaments have been suspected to be driven by hydrolysis of ATP and/or GTP [33]. More recently, ATP powered nonequilibrium fluctuations of the human red blood cell membrane have been analyzed [34] and are thought to be an important influence on cell shape. Hence metabolic energy release *per se* could justify α in the range $5 \leqslant \alpha \leqslant 10$, for instance. From the experimental results of Park *et al.* [34] one would estimate $\alpha = 2$.

The parameters contained in Eqs. (63) have been explained via the above developments with the exception of ω_0^2, which is now explained with reference to Fig. 3.

Figure 3 again illustrates our synapse model but now attached to an elastic axon, with spring constant k [Fig. 3(a)], whose segment is of length ℓ_a [Fig. 3(b)] and radius R_a (not shown to scale). The radius is taken in the range $0.5\mu \leqslant R_a \leqslant 1\mu$, and its length in the range $\ell_a \sim 100\mu$. The linear spring constant would then be formed as $k = \pi R_a^2 E/\ell_a$ and hence the expression for ω_0^2 in Eq. (63). Again, the disklike synapse is resisted by a viscous drag ξ as given in Eq. (17) that then prescribes γ in Eq. (63).

As for the elastic modulus, E, we note recent measurements of chick nerve cell elasticity obtained via AFM imaging [35,36]. For chick neurons E was reported in the range $1 \leqslant E \leqslant 10$ kPa *in vivo* [35], whereas *in vitro* E was reported in the higher range $30 \leqslant E \leqslant 90$ kPa with a strong peak at $E \approx 70$ kPa. In what follows we use a value of $E = 7$ kPa for numerical examples.

The relations in Eq. (63) can be usefully combined, for use in Eqs. (52a), (52b), (54), and (56), to yield

$$s = \frac{2}{3} E \frac{1}{\ell_a} \frac{R_a^2}{R^4} \frac{h_0^3}{\mu}, \quad \mathcal{A}^M = \beta/s = \frac{\alpha k T \ell_a}{\pi E R_a^2 h_0^2},$$

$$\mathcal{A}^D = \frac{s}{\lambda_1^2 D} = \frac{2}{15} \frac{E}{\ell_a} \left\{ \frac{R_a}{R} \right\}^2 \frac{h_0^3}{D\mu}. \tag{64}$$

We recall that Eqs. (52a), (52b), (54), and (56) demonstrate that the parameters s and β/s are pivotal for yielding an influence of advection on solute transport. Equation (56) shows that β/s, as in the term $e^{-\beta/s}$, defines the prospective "magnitude" of the net advection contribution, but s controls the timescale, $\tau_a = 1/s$, on which advection occurs. Advection is in competition with diffusion occurring with timescales $\tau_d = 1/(\lambda_n^2 D)$. Hence for advection to contribute to solute transport, $\mathcal{A}^D$ should be on the order of unity. The numerical factor in the last of Eqs. (64) is obtained by noting that $\lambda_1 R = 2.404\,68$, i.e., the first zero of $J_0(x)$. Since both s and β/s must be large enough for advection to have a noticeable influence, Eqs. (64) are seen to form a "tight box" in that varying individual parameters cannot produce arbitrarily optimal values. That is, there is indeed very little wiggle room and this feature provides additional credence to the model. Particular case examples of results from Eqs. (52a), (52b), (54), and (56) provide further insight.

B. Results for case examples

For most of our cases we set $E = 7$ kPa, $\ell_a = 100\ \mu$m, $R = 200$ nm, $R_a = 1\ \mu$m, $\mu = 10^{-3}$ Ns m^{-2}, $kT = 4 \times 10^{-21}$, $h_0 = 20{-}30$ nm, and $D = 10^{-14}{-}10^{-10}$ m^2 s^{-1}. Finally, we set $\alpha = 1{-}10$ assuming a modest additional random force input. These values specify the ranges $s \approx 250$ and $\beta/s \approx 0.25$. Also, with these values and for the values of D listed, $\mathcal{A}^D$ and $\mathcal{A}^M$ fall in the ranges $\mathcal{A}^D = 0.063{-}0.630$ and $\mathcal{A}^M = 0.0202{-}0.2021$.

Figure 4 shows $\langle \tilde{c} \rangle$ versus t for the parameters listed in each subfigure; the following observations can be made. Note that in each set of cases we show results with $D = 0$; this illustrates the potential effect of advection alone as described by Eq. (56). In this case the concentration approaches a nonzero steady-state value as time increases. This is because the randomness-related drift depends on the detailed configuration and on the particular stochastic variable that drives the process. In our problem, the specific initial conditions used in the resolution of Eq. (23) lead to the decay of randomness effect over time as measured by the stochastic variable $(1/h)dh/dt$. Varying those initial conditions will not change the essential structure or conclusions of our solution.

Clearly when diffusion is relatively fast, i.e., $D \geqslant 10^{-10}$ m^2 s^{-1}, $\mathcal{A}^D$ is too small to allow advection to contribute to solute egress from the cleftlike geometry, yet when D is as low as $D = 10^{-11}$ m^2 s^{-1}, advection has a definite effect. This can also be appreciated by observing the timescales

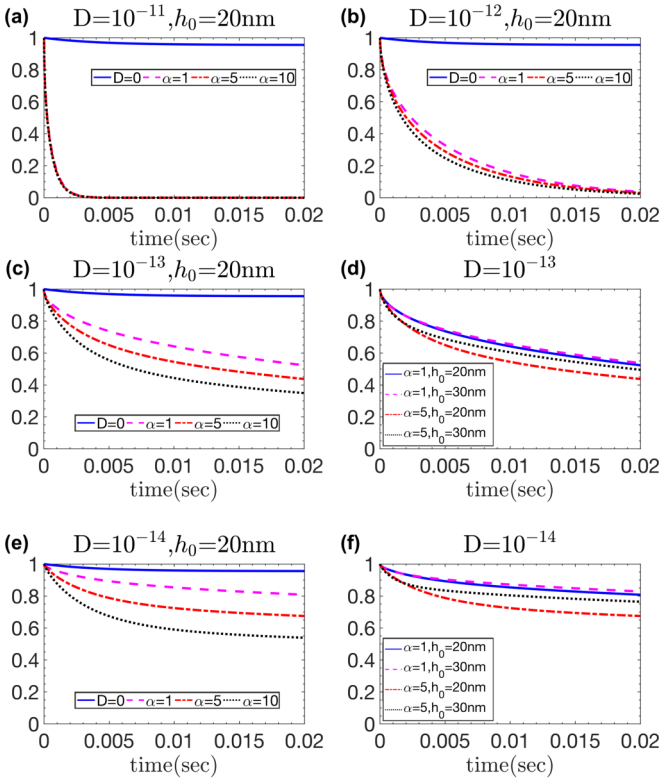

FIG. 4. $\langle \tilde{c} \rangle$ vs t for the parameters listed on each of the six panels in the figure. Note that the effective diffusion coefficient ranges from 10^{-14} to 10^{-11} m^2 s^{-1}. For the cases (a)–(c) and (e), we plot the result with $D = 0$ to more clearly reveal the effect of advection.

for measurable solute transport; with $D \geqslant 10^{-10}$ m^2 s^{-1} the timescale is on the order of 1 ms, whereas if $D \leqslant 10^{-11}$ m^2 s^{-1} timescales grow to order 10 ms. On the other hand, if $D \leqslant 10^{-12}$ m^2 s^{-1} advection is seen to have a quite noticeable effect. This is seen by the trends shown in Fig. 4(b). Thus it may be inferred that at least within the range of structural and physical properties used here, advection would contribute to transport of only larger molecules with such low diffusion coefficients.

It should be noticed, however, that additional energy input, i.e., other than via thermal fluctuations, can have the significant effect of enhancing advective flow. This is clear from the trends shown in Figs. 4(d)–4(f).

Another feature of these results is that when advection does contribute, i.e., competes with diffusion, it happens at early times. This should be clear and anticipated from the transient nature of Eq. (34). It can also be visualized by the larger slopes at short times for the cases shown in Figs. 4(c)–4(f).

V. DISCUSSION AND CONCLUSIONS

The findings of Chary and Jain in 1989 [5] should have spurred a line of further inquiry into coupled effects of advection and diffusion in biological vessels, cells, and tissue, especially given Starling's hypothesis [1] made in the 19th century. Indeed, earlier Swabb *et al.* [37] studied such effects in normal and neoplastic tissue and found that advection can dominate the flow, especially for higher molecular weight molecules. Further note the ideas put forth by Nedergaard regarding advective flow in the brain [4]. We have commented

on the fact that the fluid velocity range reported by Chary and Jain is quite comparable to what we forecast and that indeed when $D \sim 10^{-11}$ m^2 s^{-1}, we predict measurable advection contributions versus diffusion. It is informative to explore the respective forecasted pressure gradients as well. Chary and Jain report gradients of order $\partial p/\partial x \sim 4$ mm Hg/μm $\approx 5 \times 10^8$ Pa m^{-1}, where this was based on assumed values for *hydraulic conductivity*, K, extracted from other literature. The initial value they used was $K = 10^{-12}$ cm^4(dyn s)$^{-1}$ = 10^{-15} m^4(Ns)$^{-1}$. They rightly questioned if such high gradients were sustainable *in vivo* and hence proposed that the *hydraulic conductivity* could be two to three orders of magnitude higher so as to correctly lead to measured fluid velocities at more reasonable pressure gradients. If our Eq. (6) is used, as in Eq. (13), we find

$$\bar{v}_r = -\frac{h^2}{12\mu}\frac{\partial p}{\partial r} = -K\frac{\partial p}{\partial r}. \tag{65}$$

If we take $h = 20$ nm and $\mu = 10^{-3}$ Ns m^{-2} we find $K \sim 10^{-13}$ m^4(Ns)$^{-1}$, i.e., some two orders of magnitude larger that Chary and Jain's original estimate and that help verify their proposal of using larger hydraulic conductance. In fact, if we take $h \sim 60$ nm, i.e., midrange of Chary and Jain's range 30−100 nm, we find $K \sim 10^{-12}$ m^4(Ns)$^{-1}$, which is precisely what they proposed was possible. Thus our analysis indeed provides a pathway to explain, even quantitatively, experimental observations such as theirs.

We also note that our analysis shows that the effect of advection becomes significant when $D \leqslant 10^{-13}$ m^2 s^{-1} with fluid velocities of order $v \sim 0.5$ μm s^{-1} as found in Sec. III C. This forecast is consistent with the analysis of the experimental results of Koslover *et al.* [16], who report that advection effects become important for particle transport with diffusion coefficients with extracted (via their analysis) values of order $D \sim 2 \times 10^{-14}$ m^2 s^{-1}; their measured fluid velocities were, indeed, in the range $v \sim 0.5$ μm s^{-1}. This again demonstrates a consistency of our model analysis with experiment in terms of observed phenomenology and the numerology regarding key parameters such as fluid velocity and diffusion, whose values determine the competition between advection and diffusion.

Reviewing again Eqs. (64), we see that simultaneously optimizing s, β/s, and $\mathcal{A}^D$ is quite difficult. With slightly larger cleft widths, certainly verified for many types of biological channels, the timescale of advection can be shortened (i.e., quickened) so it competes more effectively with diffusion. However, this alone would reduce β/s, the magnitude of the eventual advection effect. To obtain an optimal set of values, α, i.e., additional energy input, is required. This then poses a fundamental question: How does possible metabolic energy enter into such mechanical phenomena? Is it direct or indirect, such as by participating in molecular restructuring? And, how much energy is involved and how is it triggered? Thus our model analysis indeed clearly points to the potential vital role of energetic input into biological transport processes.

Our analysis demonstrates that when advection is driven by structural motion, there are a rather rigid set of criteria that are required for it to compete with diffusion. It may be that our modeling of the synapticlike body as a rigid disk is too restraining, and explicit account should be taken of the flexible synaptic membranes. This would lead to enhanced structural motion, driving fluid motion, and increased advective solute current. This remains to be explored, especially in the context of other biological gaplike channels such as exist within the brain [4], for instance. But even here care must be taken to identify the energetic sources that drive fluid flow. Aspects of such scenarios have been addressed by Bickel [38], who has argued that random motion of opposing membranes indeed affects particle transport in viscous media.

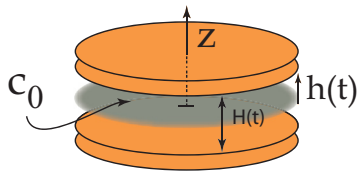

FIG. 5. Here the pre- and postsynapses are modeled as two identical opposing disks separated by $H(t) = 2h(t)$.

We also note that our finding that $\mathcal{A}^D \sim 1/R^2$ is due to the fact that structural motion that drives fluid flow is resisted by a drag coefficient that scales as $\xi \sim R^4$. Péclet numbers are often defined via dimensional analysis leading to $\mathrm{Pe} = UL/D$, with U being fluid velocity and L diffusion distance. In our case, however, U is strongly decreasing with L, and it is this that leads to our $\mathcal{A}^D \sim 1/R^2$.

Finally, we comment that our choice of random telegraph noise used to describe either $\mathcal{F}(t)$ or $\eta(t)$ was based on geometric constraints discussed in Sec. III B and that this choice provided a simple connection to thermal fluctuations via the equipartition theorem. Recall that our goal was a model scenario that would allow a clear assessment of the contributions of advection versus diffusion and its link to a set of well-defined physical parameters that mediate the system's response. As noted, however, in Sec. III B the choice of telegraph noise provides an opportunity to explore cases in which the physical system is biased in that $\langle \eta(t) \rangle \neq 0$, i.e., $\nu_1 \neq \nu_2$. Such may well be the case when the stimulus for motion is in the form of energetic bursts or pulses such as exist in the synapse, for example. This is, indeed, a topic of future research.

APPENDIX A: OPPOSING DISKS MODEL OF A SYNAPSE

Still another model for the synapse is that shown in Fig. 5, in which we envision the pre- and postsynapses as two opposing identical disks. Here we describe the disks lying at elevations $z = \pm h(t)$; hence the total gap is $H(t) = 2h(t)$. Note that now the no-slip boundary condition reads as $v_z(r, z = \pm h) = 0$. The solution to Eq. (5) is then

$$v_r = \frac{1}{2\mu}\frac{\partial p}{\partial r}(z^2 - h^2). \tag{A1}$$

Incompressibility, via Eq. (7), now leads to

$$v_z = -\frac{1}{2\mu r}\frac{\partial}{\partial r}\left(r\frac{\partial p}{\partial r}\right)\left\{\frac{z^3}{3} - h^2 z\right\}. \tag{A2}$$

Following the procedure outlined above, we find that

$$[p]^{\mathrm{in}}_{\mathrm{out}} = p(r) - p_0 = \frac{3\mu}{4h^3}\frac{dh}{dt}(r^2 - R^2)$$
$$= \frac{3\mu}{H^3}\frac{dH}{dt}(r^2 - R^2). \tag{A3}$$

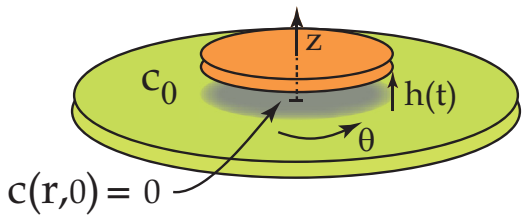

FIG. 6. The inverse problem assumes that the initial cleft concentration is $c(r,0) = 0$ and $c(R,t) = c_0$.

Comparing this to the pressure difference in Eq. (15), we find that the friction coefficient, ξ, in Eq. (17) is recovered. Moreover, the through thickness radial fluid velocity is

$$\bar{v}_r = -\frac{1}{H}\frac{dH}{dt}r, \tag{A4}$$

and thereby of the same form as in Eq. (13) as per the total cleft width of either $h(t)$ or $H(t)$.

APPENDIX B: THE INVERSE PROBLEM

The inverse problem is one in which the initial and boundary conditions are $c(r,0) = 0$ within the gap and $c(R,t) = c_0$ on the perimeter of the disk, as depicted in Fig. 6.

In such a case we write the solution in the form

$$\bar{c}(r,t) = c_0 + \sum_{m=1}^{\infty} A_m(t) J_0(\lambda_m r), \tag{B1}$$

but as opposed to Eqs. (50) and (51), invoking the initial conditions leads to

$$-c_0 = \sum_{n=1}^{\infty} A_n(0) J_0(\lambda_n r) \quad \text{and} \tag{B2}$$

$$A_n(0) = -\frac{2c_0}{(\lambda_n R) J_1(\lambda_n R)}. \tag{B3}$$

Other details are as worked out above for our original problem.

[1] E. Starling, J. Physiol. (London) **19**, 312 (1896).
[2] M. Friedman, *Principles and Models of Biological Transport*, 2nd ed. (Springer, New York, 2008).
[3] J. M. Diamond and W. H. Bossert, J. Gen Physiol. **50**, 2061 (1967).
[4] M. Nedergaard, Science **340**, 1529 (2013).
[5] S. R. Chary and R. K. Jain, Proc. Natl. Acad. Sci. USA **86**, 5385 (1989).
[6] L. P. Savtchenko and D. A. Rusakov, Proc. Natl. Acad. Sci. USA **104**, 1823 (2007).
[7] J. D. Clements, A. Robin, J. Lester, G. Tong, C. E. Jahr, and G. L. Westbrook, Science **258**, 1498 (1992).
[8] B. Corti, *Osservazione Microscopishe sulla Tremella e Sulla Circulazione del Fluido in una Planta Acquaguola. Lucca* (Appresso Giuseppe Rocchi, Lucca, Italy, 1774).
[9] W. F. Pickard, Plant Cell Environ. **26**, 1 (2003).
[10] R. E. Goldstein and J. W. van de Meent, Interf. Focus **5**, 20150030 (2015).
[11] M. Tominaga and K. Ito, Curr. Opin. Plant Biol. **27**, 104 (2015).
[12] Y. Kimura, N. Toyoshima, N. Hirakawa, K. Okamoto, and A. Ishijma, J. Mol. Biol. **328**, 939 (2003).
[13] T. Shimmen and E. Yokota, Curr. Opin. Plant Biol. **16**, 68 (2004).
[14] A. Fannjiang and G. Papanicolaou, J. Stat. Phys. **88**, 1033 (1997).
[15] L. I. Piterbarg and A. G. Ostrovskii, *Advection and Diffusion in Random Media* (Kluwer Academic, Boston, 2010).
[16] E. F. Koslover, C. K. Chan, and J. A. Theriot, Biophys. J. **110**, 700 (2016).
[17] T. A. Nielsen, D. A. DiGregorio, and R. A. Silver, Neuron **42**, 757 (2004).
[18] D. A. Rusakov, Biophys. J. **81**, 1947 (2001).
[19] K. P. Lehre and D. A. Rusakov, Biophys. J. **83**, 125 (2002).
[20] D. J. Acheson, *Elementary Fluid Dynamics* (Oxford University Press, Oxford, 1990).
[21] C. Posrikidis, *Introduction to Theoretical and Computational Fluid Dynamics* (Oxford University Press, Oxford, 1996).
[22] T. D. Bennet, *Transport by Advection and Diffusion* (Wiley, 2013).
[23] N. G. Von Kampen, *Stochastic Processes in Physics and Chemistry* (Elsevier, Amsterdam, 2006).
[24] M. Pannuzzo, A. Grassi, and A. Raudino, J. Phys. Chem. **8**, 8662 (2014).
[25] P. Tabeling, *Introduction to Microfluidics* (Oxford University Press, Oxford, 2010).
[26] A. M. J. Davis, Phys. Fluids A **2**, 301 (1990).
[27] G. Falkovich, S. Musacchio, L. Piterbarg, and M. Vucelja, Phys. Rev. E **76**, 026313 (2007).
[28] R. K. Pathria, *Statistical Mechanics* (Elsevier, Amsterdam, 2006).
[29] S. K. Ma, *Statistical Mechanics* (World Scientific, Singapore, 2004).
[30] D. Pathak, L. Shields, B. A. Mendelsohn, D. Haddad, W. Lin, A. A. Gerencser, H. Kim, M. D. Brond, R. H. Edwards, and K. Nakamura, J. Biol. Chem. **290**, 22325 (2015).
[31] V. Rangaraju, N. Calloway, and T. A. Ryan, Cell **156**, 825 (2014).
[32] D. Voet, J. Voet, and C. W. Pratt, *Fundamentals of Biochemistry* (Wiley, New York, 2001).
[33] J. Pokorný, F. Jelínek, V. Trkal, I. Lamprecht, and R. Hölzel, J. Biol. Phys. **23**, 171 (1997).
[34] Y. Park, C. Best, T. Auth, N. Gov, S. Safran, G. Popescu, S. Suresh, and M. Feld, Proc. Natl. Acad. Sci. USA **107**, 1289 (2009).
[35] E. Spedden, J. D. White, E. N. Naumova, D. L. Kaplan, and C. Staii, Biophys. J **103**, 868 (2012).
[36] M. Mustata, K. Ritchie, and H. A. McNally, J. Neurosci. Methods **186**, 35 (2010).
[37] E. A. Swabb, J. Wei, and P. M. Gullino, Cancer Res. **34**, 2814 (1974).
[38] T. Bickel, Eur. Phys. J. E **20**, 379 (2006).